Affordable amino acid α/β-deuteration and specific labeling for NMR signal enhancement: Evaluation on the kinase p38α

Rania Ghouil, Chafiaa Bouguechtouli, Hélène Chérot, Agathe Marcelot, Maxime Roche, Francois-Xavier Theillet

Journal of Magnetic Resonance Open 16–17 (2023) 100126

Contents lists available at ScienceDirect

Journal of Magnetic Resonance Open

journal homepage: www.sciencedirect.com/journal/journal-of-magnetic-resonance-open

Affordable amino acid α/β-deuteration and specific labeling for NMR signal enhancement: Evaluation on the kinase p38α

Rania Ghouil [a], Chafiaa Bouguechtouli [a,1], Hélène Chérot [a], Agathe Marcelot [a,2], Maxime Roche [b], Francois-Xavier Theillet [a,*]

[a] Université Paris-Saclay, CEA, CNRS, Institute for Integrative Biology of the Cell (I2BC), 91198, Gif-sur-Yvette, France
[b] CortecNet, 91940 Les Ulis, France

ARTICLE INFO

Keywords:
Kinase
p38
Cell-free expression
Deuteration
In-cell NMR

ABSTRACT

Although very effective in decreasing NMR relaxation of large proteins, homogeneous deuteration can be costly, and anyway unsuitable for recombinant production in metazoan systems. We sought to explore other deuteration schemes, which would be adapted to protein expression in mammalian cells. Here, we evaluate the benefits of the deuteration on alpha- and beta-positions of amino acids for a typical middle size protein domain, namely the model 40 kDa-large kinase p38α. We report the position-specific deuteration of free amino acids by using enzyme-assisted H/D exchange, executed by the cystathionine gamma-synthase and a newly designed high-performance mutant E325A. Then, we used cell-free expression in bacterial extracts to avoid any scrambling and back-protonation of the tested isotopically labelled amino acids (Ala, Leu, Lys, Ser, Asp, Glu, Gly). Our results show signal enhancements up to three in ^{1}H-^{15}N spectra when these α/β-deuterated amino acids are integrated. Because our approach relies on single $^{2}H_{\alpha/\beta}$-^{15}N-amino acid labeling, an additional three-fold increase in sensitivity is obtained by the possible use of moderate resolution SOFAST-HMQC instead of the classical HSQC or TROSY experiments. This allows recording residue-resolved solution ^{1}H-^{15}N NMR spectra of 100 μg of p38α in one hour with S/N∼10.

Introduction

Deuteration of slow-tumbling proteins is a potent strategy to decrease their NMR relaxation and, in turn, to enhance the detected NMR signal [1–3]; deuteration is thus often simply necessary to make large proteins observable by solution NMR. Protocols exist to achieve perdeuteration of recombinant proteins in *Escherichia coli* [4–6], or advanced -but not complete- deuteration in insect cells [7–11]. *E. coli* cells can grow and express recombinant proteins in 100% D_2O [12], but metazoan cells cannot [13–15]. Insect cells can be maintained in 100% D_2O in an NMR tube during spectra acquisition, while mammalian cells suffer above 60% D_2O [16–18]. Cultured mammalian cells stop growing at D_2O levels above 30 to 50% [19–23], depending on the cell lines, even though a successful expression of GFP in HEK cells was reported once at 70% D_2O -without any evaluation of deuterium integration [16]. Hence, to the best of our knowledge, advanced deuteration in mammalian cells has not been achieved, even though ^{2}H-Arg-, -Lys-, -Met- or -Leu-labeling have been reported for quantitative proteomics purposes [24–29], and ^{2}H-Leu-labeling for methyl-NMR investigations of antibodies [30]. More thorough deuteration would probably be anyway expensive in mammalian cells: like insect cells, those require culture media supplemented with mixes of essential amino acids, which are commercialized or home-produced at high cost in their ^{15}N-only labeled version (between 2,000 and 10,000 euros/L) [31–33].

Expressing proteins in mammalian cells is becoming almost a routine in both industry and academia (e.g. contributing for about 15, 150 and 1500 structures in the PDB in 2003, 2012 and 2022), giving rise to intense efforts to improve production yields [34–37]. New isotope labeling approaches in mammalian cells, including deuteration, should be developed for making NMR spectroscopy likely to contribute in many modern questions in biophysics and biochemistry. We have notably in mind our long-term goals in making in-cell NMR investigations more amenable for a broader range of targets [18,38]. Here, we sought to evaluate some deuteration schemes in regards to their capacity to

* Corresponding author.
E-mail address: francois-xavier.theillet@cnrs.fr (F.-X. Theillet).
[1] Present address: Structural Motility, Institut Curie, Paris Université Sciences et Lettres, Sorbonne Université, CNRS UMR144, 75005 Paris, France.
[2] Present address: Expression Génétique Microbienne, UMR 8261, CNRS, Université Paris Cité, Institut de Biologie Physico-Chimique (IBPC), 75005, Paris, France.

https://doi.org/10.1016/j.jmro.2023.100126

Available online 9 July 2023

improve two-dimensional ^{1}H-^{15}N NMR spectroscopy at the widespread 600–700 MHz magnetic fields. At these fields, ^{1}H-^{1}H dipolar relaxation has dominating contributions on the T2 relaxation of the detected amide $^{1}H_N$ nuclei. Deuteration in their vicinity should thus have interesting benefits on signal intensities.

Inspired by recent reports from Shimada and colleagues [7,11,39–41], we sought to explore in particular the practical NMR consequences of deuteration in α- and β-positions of amino acids for a model drug target, the kinase p38α [42]. Such deuterated amino acids can indeed be obtained by H/D exchange catalyzed by the bacterial cystathionine gamma-synthase (CGS), as shown by LeMaster and colleagues [43]. We designed a mutant E325A, which proved to have superior capacities in catalyzing α/β H/D exchange for amino acids Glu, Lys and Arg. We also evaluated the effects of specifically α-deuterated amino acids produced by chemical catalysis [44,45]. We supplemented $^{2}H_{\alpha}$-^{15}N or $^{2}H_{\alpha\text{-}\beta}$-$^{15}N$ amino acids in a bacterial cell-free expression system, hence avoiding any isotopic scrambling [46,47]. This provided specifically $^{2}H_{\alpha\text{-}\beta}$-$^{15}N$ labeled p38α samples, allowing the first accurate quantification of the benefits of α/β-deuteration on $^{1}H_{amide}$ NMR relaxation and signal.

Together with employing ^{1}H-^{15}N SOFAST-HMQC pulse sequences, such $^{2}H_{\alpha\text{-}\beta}$-$^{15}N$ amino acid-specific labeling permits the acquisition of spectra at signal-to-noise ratios about 10 in one hour for p38α concentrations at 25 μM in 100 μL, i.e. 100 μg, at 600–700 MHz.

Materials and methods

Chemical α-deuteration of amino acids

$^{2}H_{\alpha}$-^{15}N-Alanine, $^{2}H_{\alpha/\beta}$-^{15}N-Serine, $^{2}H_{\alpha}$-^{15}N-Lysine, $^{2}H_{\alpha}$-^{15}N-Leucine were obtained by stereoretentive deuteration of protonated amino acids, using Ruthenium-catalyzed H/D exchange according to protocols published earlier [44,45]. $^{2}H_{10}$-^{15}N-Leucine was purchased from Eurisotop.

Enzyme-assisted α/β-deuteration of amino acids

α/β-deuteration was carried out using the approach described earlier by LeMaster and collaborators [43].

The cystathionine gamma-synthase (CGS) was produced recombinantly in *E. coli* BL21(DE3)Star, using an optimized gene synthesized and cloned into a pET-28a(+) vector by Genscript. The designed construct contained a His6-tag and a Tev cleavage site. The expression was induced at an OD=0.8 by IPTG at 0.25 mM, and carried out at 310 K during 4 h. After cell lysis by sonication in Tris at 20 mM, NaCl at 150 mM, DTT at 5 mM and PMSF at 1 mM (pH 7.5), and centrifugation at 15,000 g during 15 min, the soluble fraction was purified using a two-steps procedure: the lysate was loaded on a Ni-NTA resin column (His-Trap FF, Cytiva); fractions containing the protein of interest were then concentrated, and submitted to a final size-exclusion chromatography (Superdex 16/60 200 pg, Cytiva) previously equilibrated with phosphate at 20 mM, NaCl at 150 mM, at pH 7.4. CGS-WT and CGS-E325A were eluted at a volume of ~70 mL, consistent with the native tetrameric form that ensures a catalytic activity. The protein was finally concentrated at about 1 to 2 mM and lyophilized, then resuspended in D_2O.

For deuterating Lys, Arg, Asp and Glu, we used a version of CGS alanine-mutated at position 325 (E325A): although less stable, this mutant is more efficient for deuterating the above-mentioned amino acids. CGS-E325A is prone to release PLP faster than CGS-WT.

α/β-deuteration was performed at 310 K, or 303 K when mentioned. Amino acids of interest were solubilized in D_2O (99% D_2O, 1% H_2O), buffered with phosphate at 20 mM, pH 6.8 +/- 0.1, then lyophilized and re-dissolved in D_2O. Residual HOD ^{1}H resonance from the D_2O solvent was used to reference chemical shift, according to IUPAC recommended method: HOD chemical shift from DSS was δ_{HOD}=4.766-(310–298) *0.0119–0.009=4.614 ppm, according to Wishart et al. and considering a salt concentration of 100 mM [48].

Deuteration kinetics were monitored by recording interleaved 1D ^{1}H and natural abundance 2D ^{1}H-^{13}C edited-HSQC spectra at 600 MHz or 700 MHz spectrometers, equipped with $^{1}H/^{13}C/^{15}N$ cryoprobes TXI and TCI, respectively. (1D ^{13}C and ^{13}C-dept spectra were also recorded when monitored at 700 MHz). The analysis was carried out by integrating peak area in 1D spectra; these were plotted in Kaleidagraph 5 (Synergy Software), where the curves were fitted using the equation I(t)=*A**exp(-K*t)+*B*, with A, K and B the fitted parameters. Fig. 3 and S3 were then edited using Affinity Designer (Serif).

Altogether, every CGS-catalyzed H/D exchange requires about 2–3 h of bench work, and about 3 lyophilization steps in D_2O, i.e. ~5 mL of D_2O for 10 to 100 mg of the amino acid of interest, depending on its solubility. The bench work to produce the CGS enzyme should also be included in the global cost; it requires about one day for the purification of ~100 mg of protein from 4 L of culture.

Theoretical estimation of transverse dipole-dipole component in $^{1}H_N$-T2 relaxation

We added hydrogen atoms to crystal structures of p38α (PDB: 3HLL) and Cdk1 (PDB: 4YC6) using Pymol (Schrödinger). For every amide Leu-$^{1}H_N$ or Lys-$^{1}H_N$, we listed all ^{1}H nuclei closer than 3.5 Å to the considered $^{1}H_N$. Then, we used a rigid structure model, where the dipolar component $R2_{dd}(^{1}H_N)$ is the sum of all ^{1}H–^{1}H dipole-dipole contributions, which are proportional to $b^2 = \sum_j \frac{1}{(d(H_N-H_j))^6}$, with d($H_N$-$H_j$) the distance between $^{1}H_N$ and its close neighbor $^{1}H_j$ [49,50]. Indeed, for the sake of simplicity in the context of a rough statistical evaluation, we neglected all variations due to local order parameters and conformational exchange at any time scale or due to water-amide proton exchange. Hence, the relative contribution from every $^{1}H_j$ to the transverse dipole-dipole relaxation of $^{1}H_N$ was simply calculated from the ratio d(H_N—H_j)$^{-6}/b^2$. Fig. 2 was plotted in Kaleidagraph 5 (Synergy Software) and edited using Affinity Designer (Serif).

Recombinant production of isotope-labeled p38α

Recombinant p38α was produced using BL21(DE3)Star *E. coli* transformed with a plasmid pET-41a(+) containing an optimized gene coding for a construct His6-Tev-p38α (synthesized and cloned by Genscript, the gene coding for GST, which is present by default in pET-41a (+), was excised). The extra-N-terminal peptide was MKGSHHHHHHSAGENLYFQG-. This gene was also used for cell-free expression but cloned into a pIVEX2.3 vector by Genscript. After clonal selection and precultures in LB, cells were grown at 37 °C in M9 medium supplemented with 50 μg/mL kanamycin, and containing $^{15}NH_4^+$ (0.5 g/L) as sole source of nitrogen for ^{15}N-labeling. For $^{13}CH_3$ labeling of the isoleucine (δ1) methyl groups in a $^{2}H/^{12}C$ background, cells were progressively adapted to D_2O in LB culture media integrating stepwise-increasing D_2O concentrations [4], and finally grown in 99%-D_2O-based M9 medium containing 2 g/L of [*u*-^{2}H]-glucose (Cortecnet) and 70 mg/L of [methyl-^{13}C, 3,3–$^{2}H_2$]-α-ketobutyric acid (Eurisotop).

Overexpression was induced at an optical density OD600=0.8 by supplementing the medium with ITPG at 0.25 mM, incubated at 30 °C during 4 h or overnight in H_2O- and D_2O-based M9 media, respectively. Cells were harvested by centrifugation 4 h later and cell pellets stored at −80 °C. Cell lysis was performed using sonication in Tris at 20 mM, NaCl at 150 mM, pH 7.5 (TBS) in presence of benzonase, lysozyme, protease inhibitors 1x (EDTA-free cOmplete, Roche) and DTT at 10 mM. Soluble and insoluble fractions were separated using 15 min centrifugation at 15,000 g. The soluble fractions were then submitted to the purification protocol described below.

Cell-free protein expression and amino acid-specific isotope labeling of p38α

Cell-free expression kits "Musaibo Kun" were kindly provided by Taiyo Nippon Sanso; these kits permit coupled transcription and translation using the T7RNA polymerase and a S30 bacterial extract [46, 51–54]. The cell-free expression was carried out in H_2O solvent, using either natural abundance amino acids supplemented with a 10-fold excess (i.e. at a concentration of 20 mM) of the isotopically labeled amino acid of interest; a commercial mix of [^{2}H-^{15}N] amino acids (Taiyo Nippon Sanso) was used for producing the perdeuterated p38α. These kits contain the adequate inhibitors avoiding scrambling and back-protonation of most of the deuterated amino acids [46,51–54]. The cell-free expression was executed using 1 mL of S30 bacterial extract (internal solution, reaction mixture) in dialysis exchange with 10 mL of a feeding mix (external solution) containing notably amino acids and dNTPs. 10 μg of a pIVEX2.3 plasmid containing a gene coding for His6-Tev-p38α were spiked in the internal solution, and the expression was carried out under gentle shaking overnight at 303 K.

The optimized gene was synthesized by Genscript and inserted in the pIVEX2.3 vector at NdeI and AvrII cloning sites. Several versions of the coding gene were tested to avoid stable RNA secondary structures in the vicinity of the Ribosome Binding Site and the Methionine start codon; this proved to be key for improving the production yields (Fig. S6), in agreement with recent reports from Kigawa and colleagues [55]. The RNA secondary structures thermodynamic ensembles were predicted using the RNA fold webserver (http://rna.tbi.univie.ac.at/cgi-bin/RNAWebSuite/RNAfold.cgi) [56]. pIVEX2.3 was purchased from Biotechrabbit. The reaction mixture was harvested in the morning, spun 5 min at 14,000 g and the supernatant was submitted to the purification steps described below. Final protein yields after purification were about 0.5 to 1 mg per mL of cell-free reaction mixture (i.e. internal solution).

Purification and sample preparation

All samples were prepared following the same protocol. A first His-trap chromatography was achieved, by loading cell lysates (for recombinant production) or cell extracts (for cell-free expression) on a Ni-NTA resin column (His-Trap FF 5 mL, Cytiva); fractions containing p38α were then concentrated after addition of DTT at 2 mM and protease inhibitors (cOmplete EDTA-free, Roche), and submitted to a final size-exclusion chromatography (Superdex 16/60 75 pg, Cytiva) previously equilibrated with phosphate at 20 mM, NaCl at 150 mM (considered to be phosphate buffer saline, PBS), at pH 7.4. The purification was achieved at 277 K. The sample was then concentrated after supplementing with $MgCl_2$ at 5 mM and DTT at 2 mM. The final protein concentration was between 50 and 200 μM. The samples were immediately used for NMR analysis or stored at −20 °C. p38α inhibitors VX-375 and PH-797804 were purchased from Sigma-Aldrich, and dissolved at 14 mM in deuterated DMSO (Eurisotop). They were further diluted at 1.4 mM in deuterated DMSO, before mixing at 1.1:1 inhibitor:p38α ratios in final samples, for p38α concentrations ranging from 20 to 50 μM.

NMR acquisition, processing and analysis of p38α samples

The present NMR spectra were recorded on a 700 MHz Bruker Avance Neo spectrometer, equipped with a cryogenically cooled triple resonance ^{1}H[^{13}C/^{15}N] probe optimized for ^{1}H detection (TCI Bruker from 2006: ^{1}H 0.1% ethylbenzene $S/N = 7260$ when delivered). Spectra were recorded using 3 mm diameter Shigemi tubes, in samples supplemented with DSS (final concentration about 100 μM) and 3% D_2O. The concentration of p38α ranged from 50 to 200 μM, except for samples supplemented with inhibitors, where p38α was at 25 μM.

The pulse programs from the Bruker library were used, namely hsqcetfpf3gpsi2 for the ^{1}H-^{15}N seHSQC experiments, trosyetf3gpsi.2 for the ^{1}H-^{15}N seTROSY experiments, sfhmqcf3gpph for the ^{1}H-^{15}N SOFAST-HMQC experiments (using a Reburp refocusing pulse instead of the r-Snob set by default in the pulse program, in agreement with Schanda and colleagues [57]), and sf_metrosygpph for the ^{1}H-^{13}C SOFAST-methyl-HMQC. The angle of excitation was always 90°

The ^{1}H-^{15}N seHSQC, the ^{1}H-^{15}N seTROSY and the ^{1}H-^{15}N SOFAST-HMQC experiments were carried out with 1536 (^{1}H) x 128 (^{15}N) complex points and sweep widths of 16.23 ppm (^{1}H) and 36 ppm (^{15}N), and interscan delays of 1 s. The ^{1}H-^{13}C SOFAST-methyl-HMQC experiments were carried out using 2048 (^{1}H) x 92 (^{13}C) complex points and sweep widths of 14.87 ppm (^{1}H) and 9 ppm (^{13}C), and interscan delays of 0.3 s. For determining apparent T1* relaxation rates, we also recorded: ^{1}H-^{15}N seTROSY spectra with interscan delays of 0.6, 1, 2 and 3 s; ^{1}H-^{15}N SOFAST-HMQC spectra with interscan delays of 0.2, 0.3, 0.4, 0.5, 0.6, 0.8, 1.2 and 1.8 s; ^{1}H-^{13}C SOFAST-methyl-HMQC spectra with interscan delays of 0.04, 0.07, 0.1, 0.2, 0.3, 0.4, 0.5, 0.6, 0.8, 1, 1.5 and 3 s; up to 128 dummy scans were used for the shortest interscan delays. The number of scans ranged from 8 to 64, depending on the used concentrations of protein and on the interscan delay.

All spectra were processed in Topspin 4.0.4. Different types of processing were used depending on the application. For the Signal-to-noise ratio per molar per unit of time (S/N-PMUT) and T1* measurements of single amino acid labeled samples (i.e. integrating ^{1}H-, or $^2H_\alpha$, or $^2H_{\alpha/\beta}$-, or $^2H_{10}$- and ^{15}N-labeled Ala, Lys or Leu) in ^{1}H-^{15}N SOFAST-HMQC and ^{1}H-^{15}N seTROSY spectra, the FIDs were truncated at 768 and 92 complex points, and transformed using qcosine and cosine window functions in the ^{1}H and ^{15}N dimensions, respectively. These settings were also used for the Figures presenting spectra of single amino acid labeled samples. For S/N-PMUT measurements of uniformly ^{15}N-labeled samples in ^{1}H-^{15}N spectra, the FIDs were truncated at 1028 complex points in the ^{1}H dimension (using the 128 recorded points in the in the ^{15}N dimension), and transformed using a cosine window function in both the ^{1}H and ^{15}N dimensions. These settings were also used for the Figures presenting spectra of the uniformly ^{15}N-labeled samples. For the S/N-PMUT and T1* measurements of [u^2H-^{1}H/$^{13}C_{\delta1}$-Ile]-p38α in ^{1}H-^{13}C SOFAST-methyl-HMQC spectra, the FIDs were transformed using a cosine window function in the ^{1}H dimension. S/N-PMUT were calculated based on the acquisition time corresponding to the number of increments in the ^{15}N dimension after FID truncation. For determining the ^{1}H-linewidth at half height in ^{1}H-^{15}N spectra, the FIDs were transformed using no window function in the ^{1}H dimension and a cosine (or a qcosine in the case of single amino acid labeled samples) window function in the ^{15}N dimension. For determining the ^{1}H-linewidth at half height in ^{1}H-^{13}C spectra, the FIDs were transformed using no window function in the ^{1}H dimension and a cosine window function in the ^{13}C dimension.

Peak intensities and ^{1}H-linewidths in two-dimensional ^{1}H-^{15}N and ^{1}H-^{13}C spectra were measured in CcpNMR Analysis 2.4. ^{1}H-linewidths were obtained by the automatic fitting of the peak lineshapes using a Lorentzian function. Only well-separated peaks were selected. Noise levels were evaluated from 100 random points manually picked in spectra using CcpNMR Analysis 2.4. The root mean square of the 100 intensities was defined as the spectral noise.

Signal-to-noise ratio per molar per unit of time (S/N-PMUT) was defined as $S/N\text{-}PMUT=(S/N).[p38\alpha]^{-1}.(n*T_{scan})^{-1/2}$ with n the number of scans and T_{scan} being the total experimental time for a single scan, i.e. $T_{pulse\text{-}seq.}+T_{acq}+T_{interscan}$, in agreement with the recommendations from Schanda et al. [57].

The apparent recovery times T1* were obtained from fitting the buildup curves of isolated peaks using the equation $I(T_{scan})=I_0*(1-\exp(-T_{scan}/T1*))$.

The residue-specific analysis benefitted from the assignments previously released by Schwalbe and colleagues, and Peti and colleagues (BMRB: accession numbers 6468 and 17471) [58–60], and the Ile-δ1 methyl assignment from Tokunaga et al. (BMRB: accession numbers 19930) [61].

Data in Figs. 1 and 4 were plotted in Kaleidagraph 5 (Synergy Software) and edited using Affinity Designer (Serif). Spectra were exported

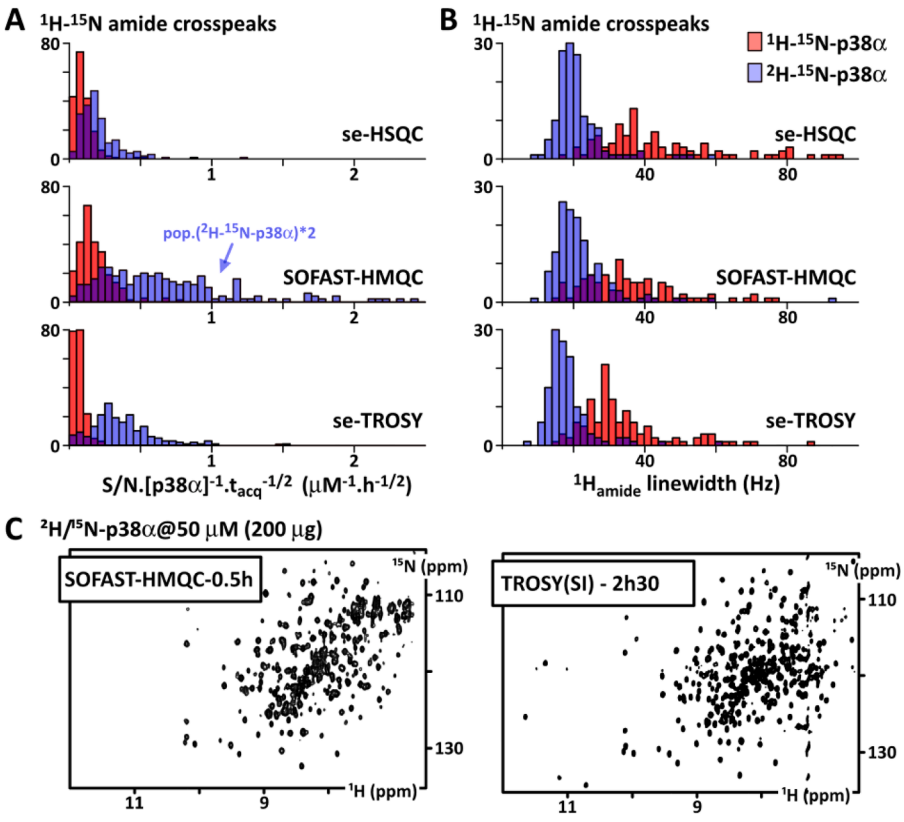

Fig. 1. A. S/N-PMUT distribution among crosspeaks of fully protonated (red) and perdeuterated (blue) p38α in two-dimensional ^{1}H-^{15}N spectra using se-HSQC, SOFAST-HMQC and se-TROSY pulse sequences; the population is very scattered for the SOFAST-HMQC, so we doubled the height of the histogram for the sake of visibility; B. Statistics for $^{1}H_{amide}$-linewidth at half-height of well-separated crosspeaks obtained in the same conditions than in A; C. ^{1}H-^{15}N SOFAST-HMQC and se-TROSY spectra obtained from perdeuterated [*u*-^{2}H/$^{1}H_{amide}$/^{15}N]-p38α produced using deuterated amino acids and cell-free expression in H_2O; both spectra are shown using contours visible from 4 times the average noise level. More spectra are shown in Figure S1.

from Topspin 4 (Bruker) and edited using Affinity Designer (Serif).

Results

Prior evaluation of NMR sensitivity and linewidth in ^{1}H-^{15}N 2D spectra for p38α

As a prior step in our NMR investigations on kinases, we determined the sensitivities and resolutions generated from ^{15}N-labeled p38α analyzed using standard ^{1}H-^{15}N pulse sequences from the Bruker pulse programs library. We selected the sensitivity-enhanced HSQC (se-HSQC) [62], SOFAST-HMQC [57] and sensitivity-enhanced TROSY (se-TROSY) [63], and recorded spectra in a close-to-physiological PBS buffer, at 700 MHz and 298 K. These measures give good hints about the residue-scale information accessible in ^{1}H-^{15}N two-dimensional spectra for a ^{15}N-labeled Ser/Thr-kinase domain, whose correlation time is expected to be about 30 ns [64]. Other useful versions of HSQC and TROSY exist [65–69], some of which can further enhance sensitivity up to a factor 2–3 by better controlling longitudinal magnetization and its relaxation [70–75]. Their evaluation will be the subject of later reports: here, we focused on $^{1}H_N$-T2-relaxation and the impact of α-β-deuteration.

We compared sensitivity and $^{1}H_N$-linewidth at 700 MHz for samples containing either the recombinant, fully protonated p38α, or the perdeuterated p38α from cell-free expression (Fig. 1). Using perdeuterated amino acids and adequate inhibitors of transaminases, commercial cell-free expression kits permit to produce proteins with >97% deuteration of alkyl positions, but 100% protonation of amide functions [46,47,51–54].

We observed that the ^{1}H-^{15}N SOFAST-HMQC pulse sequence delivered the highest signal-to-noise ratios per molar per unit of time (S/N-PMUT) both for protonated and perdeuterated p38α, using adapted spectral sweep-widths and a maximum ^{15}N-chemical shift evolution time $t1_{acq}^{max}$ of 25 ms (Fig. 1). We must mention that the ^{1}H-^{15}N SOFAST-HMQC selective pulses were set up to maximize signal intensities of peaks resonating between 6.5 and 10.5 ppm in the ^{1}H-dimension, hence sacrificing a few peaks above 10.5 ppm. Our S/N evaluation were thus carried out on crosspeaks in the region 6.5 ppm < δ(^{1}H) < 10.5 ppm. Interestingly, the SOFAST-HMQC experiment benefitted of an average ~3-fold increase in S/N-PMUT between [*u*-^{1}H]- and [*u*-^{2}H/$^{1}H_N$]-p38α, while the se-HSQC experiment gains were only ~2. This can be explained by the fact that the ^{15}N chemical shift evolution develops under a $^{1}H_N$-T2+^{15}N-T2 relaxation in the HMQC scheme, and only under the ^{15}N-T2 relaxation in the HSQC approach [57]. Consistently, the deuteration of positions neighboring the $^{1}H_N$ has thus a greater effect when using the HMQC framework: in the fully protonated p38α, the well-separated peaks have an average $^{1}H_N$-linewidth at half-height of ~40 Hz corresponding to $^{1}H_N$-T2~8 ms, which results in about 85% losses in coherent magnetization during the 15 ms-long SOFAST-HMQC pulse sequence; perdeuteration makes $^{1}H_N$-linewidth twice sharper, i.e. an average $^{1}H_N$-T2 of about 15 ms and only 60% of coherent magnetization is lost during the same pulse sequence (of course, these losses grow when time is given for ^{15}N chemical shift evolution).

This gain was such that the ^{1}H-^{15}N SOFAST-HMQC surpassed also the ^{1}H-^{15}N se-TROSY for both isotopic labeling schemes at 700 MHz. The TROSY approach generates naturally sharper peaks and better resolved spectra, which contain consequently more information than their SOFAST-HMQC counterparts.

In the context of our study, aiming at testing amino acid-specific labeling schemes and α/β-deuteration, we thought that the ^{1}H-^{15}N SOFAST-HMQC would give access to a more straightforward and accurate quantification of the differences between fully protonated p38α and later deuterated versions. Moreover, amino acid-specific labeling results in much less crosspeaks in two-dimensional spectra, hence permitting the use of lower resolutions in the ^{15}N-dimension with $t1_{acq}^{max}$ of about 10 ms. This would favor the sensitivity of the ^{1}H-^{15}N SOFAST-HMQC even more: shorter $t1_{acq}^{max}$ is also favorable for ^{1}H-^{15}N se-TROSY, but its S/N-PMUT benefits less of a lower ^{15}N-resolution than ^{1}H-^{15}N SOFAST-HMQC, because of the ^{1}H-^{15}N se-TROSY slower relaxation in the ^{15}N-

dimension.

Theoretical evaluation of protons contributions to T2 relaxation and NMR signal in kinases

Transverse ^{1}H–^{1}H dipolar relaxation is proportional to $d_{(1H\text{-}1H)}^{-6}$, with $d_{(1H\text{-}1H)}$ the distance between the considered protons. The proton $^1H\alpha_{i\text{-}1}$ is often the closest to the detected $^1H_{Ni}$: $d(^1H\alpha_{i\text{-}1}–^1H_N)$~2.25–2.5 Å in β-strands, and ~3.5 Å in α-helices; $^1H_{Ni\text{-}1}$ or $^1H\beta_{i\text{-}1}$ can also be at ~2.5 Å from $^1H_{Ni}$ in α-helices and β-strands, respectively [76,77]. This would argue for deuterating preferentially i-1 residues, which is more achievable by uniform labeling than by amino acid-specific approaches. However, the 260 to 400 residue-long Tyr-Ser-Thr-kinase domains (Fig. S2) have high α-helical contents of about 50% (among which the scaffolding F-helix and the regulatory C-helix) and low β-sheet contents (~15%, mostly in the N-lobe) [78,79]. As an example, the 360-residue--long p38α contains 170 residues in α-helices and only 45 residues in β-strands.

Using crystal structures and a rough model of transverse dipole-dipole relaxation omitting conformational flexibility and water-amide proton exchange, we estimated the statistics of the contributions of $^1H\alpha_{i\text{-}1}$, $^1H\alpha_i$, $^1H\beta_i$ on the dipolar component of ^1H_N-T2 for two representative amino acids, namely Lys and Leu, in two kinases, namely p38α and Cdk1 (Fig. 2). We chose these amino acids because they are frequent enough to obtain decent statistics on the effects of α/β-deuteration, and also because they permitted to evaluate different types of β- or even γ-deuteration in the case of Leu.

These calculations show that $^1H\alpha_{i\text{-}1}$ of Leu and Lys have often more impact on ^1H_N-T2 than $^1H\alpha_i$ do. However, the $^1H\beta_i$ have even higher contributions in a number of instances for Lys and Leu. Overall, these predictions argue in favor of our strategy, i.e. integrating α/β-deuterated amino acids to decrease ^1H_N-T2 relaxation and enhance the ^1H-^{15}N NMR signal.

Cystathionine gamma-synthase (CGS) WT and E325A for α/β-deuteration of free amino acids

LeMaster and colleagues have shown, 30 years ago, that the

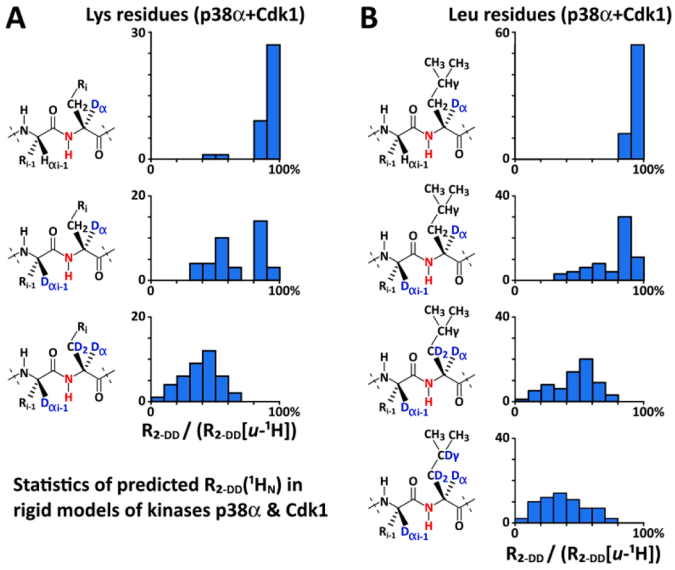

Fig. 2. Distributions of the predicted dipole-dipole component of the transverse relaxation for amide protons $R_{2\text{-}DD}(^1H_N)=1/(^1H_N\text{-}T_2)$ of A. Lysine and B. Leucine residues in p38α and Cdk1, depending on the deuteration scheme of these amino acids; the calculation was performed based on crystal structures of these kinases, and using a simplified model of rigid molecules, where relaxation is only related to proton-proton distances.

Cystathionine Gamma-Synthase (CGS) from *E. coli* could catalyze H/D exchange at the α-, and sometimes also at the β-positions of a number of amino acids [43]: protonated amino acids dissolved in D_2O are thus progressively turned into α-, or α/β-deuterated amino acids, in presence of CGS (Fig. S3A). We designed an optimized gene for the recombinant overproduction of CGS in *E. coli*. After purification, lyophilization and resuspension in D_2O, our version of CGS revealed its catalytic capacities in H/D exchange on free amino acids (Fig. 3, Fig. S3, Table S1), showing preferences very similar to those reported by LeMaster et al. [43]. CGS is potent at varying degrees for H/D exchange i) at α-positions of free amino acids, except for Thr, Phe, Tyr, Trp and Val, and ii) at one of the two β-protons of hydrophilic amino acids with strong chiral preferences (except for Ser, whose β-protons are both rapidly exchanged).

In our hands, this activity is always present but its efficiency is not

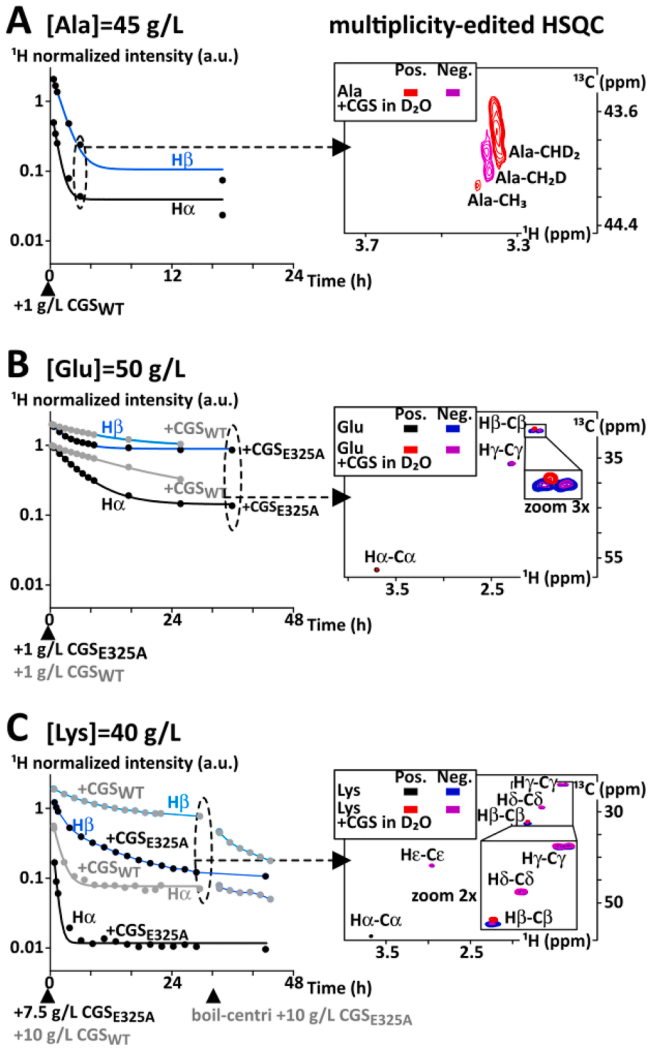

Fig. 3. A. *Left:* Time course of the progressive decrease in peak intensity of NMR signals from Hα (black) and Hβ (blue) of free Alanine in presence of CGS_{WT}; *Right:* Close-up view of a multiplicity-edited HSQC spectrum recorded after 3 h of incubation at 37 °C, showing the NMR signals from the mono-, di- and tri-protonated methyls of Alanine remaining in the sample. This is consistent with a non-processive enzymatic mechanism. B. *Left:* Time course of the progressive decrease in peak intensity of the NMR signals from Hα (black and gray) and Hβ (blue and sky blue) of free Glutamate in presence of CGS_{E325A} (black and blue) and CGS_{WT} (gray and sky blue); *Right:* Overlay of multiplicity-edited HSQC spectra recorded at time 0 and after 35 h of incubation, showing notably the chiral preferences of CGS among the two Hβ of Glutamate for H/D exchange. C. Same than in B., but with Lysine. In multiplicity-edited HSQC spectra, signals from -CH and -CH_3 are positive, those from -CH_2 are negative.

fully reproducible from batch to batch: the yellow color of CGS, due to the complexation of pyridoxal 5′-phosphate (PLP) necessary for the catalytic activity, was of varying intensity depending on the batches, and it correlates with CGS catalytic power. Consistently, the progressive release of PLP at 310 K is observable in the test tube by the loss of the yellow color (we did never observe any CGS precipitation). This affects the amino acids' deuteration build-up curves, which are not exactly mono-exponential because of the progressive exhaustion of CGS activity (Fig. 3A-B). Moreover, the remaining protons from the lyophilized CGS and protons released from the concentrated free amino acids (at 0.1 to 1 mol.L^{-1}) upon H/D exchange are responsible for deuteration plateauing below 95%. Hence, to obtain deuteration levels superior to 95%, we had to perform more than two rounds of H/D exchange in D_2O in presence of CGS: once deuteration was no longer progressing, we boiled the sample to precipitate the unactive CGS, and then performed a lyophilization step, resuspended the free amino acid in D_2O and supplemented the sample with fresh CGS (see Fig. 3C, and Fig S3E-F-G).

Then, based on a structural analysis (PDB: 1CSB), we designed mutants of the bacterial CGS that would present a larger and less negatively-charged enzymatic cavity, in order to make them more efficient for a broader range of amino acids. We produced CGS-D45A and CGS-E327A unsuccessfully: they released PLP very soon and did not present any strong catalytic activity. At the opposite, CGS-E325A showed exacerbated capacities in H/D exchange for charged amino acids Glu, Lys and Arg (Fig. 3B-C, Fig S3E-I): CGS-E325A was about 3 times more efficient than CGS-WT for Glu, 2 times for Lys and 7 times for Arg, both for α- and β-protons in all these cases (see Table S1). CGS-E325A does not appear to offer better capacities for the other amino acids, and it releases PLP faster than its WT counterpart at 310 K, although it looks about equivalently stable at 303 K (Fig. S3H). Despite lower stability and activity, CGS-E325A is anyway worth using in the catalysis of H/D exchange of the charged amino acids Asp, Glu, Lys and Arg.

Hence, using CGS-WT or CGS-E325A, we could produce tens of milligrams of α-deuterated Gly, Leu and Val, and α/β-deuterated Ala, Asp, Glu, Lys, Arg and Leu, either ^{14}N- or ^{15}N-labeled. Their production was more affordable than purchasing commercial uniform ^{2}H-^{15}N-amino acids, which are on average 4 times more expensive than their ^{15}N-counterparts (see Table S2). We used them later for cell-free expression and isotope labeling of p38α: we used commercial amino acid mixes (from the cell-free expression kits), supplemented with a 10-fold excess of the chosen deuterated amino acids, ensuring a ~90% α/β-deuteration and/or ^{15}N-labeling of the corresponding residues in the produced protein without isotopic dilution or back-protonation [46, 51–54].

Evaluation of sensitivity and relaxation in ^{1}H-^{15}N 2D SOFAST-HMQC of α- or α/β-deuterated p38α

We produced various isotope-labeled versions of p38α, using cell-free expression in presence of the $^{2}H_{\alpha/\beta}$- and/or ^{15}N-labeled Ala, Lys and Leu. We recorded ^{1}H-^{15}N SOFAST-HMQC spectra at 600 and 700 MHz at 298 K, using a range of interscan delays from 0.2 to 1.8 s. We obtained results at 600 MHz very similar to those reported here at 700 MHz, but the set of data at 600 MHz is less complete and was generated using two different cryoprobes (breakdown issues, data not shown).

Then, we measured the signal intensities, the $^{1}H_N$ linewidth and the apparent T1* relaxation for every resolved crosspeak in the ^{1}H-^{15}N SOFAST-HMQC spectra (Fig. 4A). The experimental results were very consistent with the predicted effects of α/β-deuteration on $^{1}H_N$-T2 (Fig. 2): the α-deuteration provoked signal gains of 10% except in the case Ala-Ala, Lys-Lys or Leu-Leu motifs, for which signal intensities doubled because of the α-deuteration in position i-1 (Figs. 4A, 5); the α/β-deuteration permitted to get 10 to 20% more signal on ^{1}H-^{15}N crosspeaks, and was a bit more efficient for Lys-residues; the full deuteration of Leu-residues produced an average 60% gain in signal.

As expected, the α-deuteration in position i-1 has often important benefits on $^{1}H_{Ni}$ S/N-PMUT (Fig. 4A). We thought to integrate $^{2}H_{\alpha/\beta}$-^{14}N-Asp, $^{2}H_{\alpha/\beta}$-^{14}N-Glu, $^{2}H_{\alpha/\beta}$-^{14}N-Gly and $^{2}H_{\alpha/\beta}$-^{14}N-Lys together with $^{2}H_{\alpha/\beta}$-^{15}N-Leu in p38α: Asp-, Glu-, Gly-or Lys-residues are found 16 times in position i-1 of Leu-residues in the primary structure of p38α, 11 of those Leu generating well-resolved, assigned cross-peaks. Satisfyingly, six of these peaks showed 2- to 3-fold S/N-PMUT enhancements in this last labeling scheme (Figs. 4A, 5). Overall, we evaluated that the improvement in S/N-PMUT was above 1.5 for 16 out of 19 amino acids with an α-deuterated amino acid in position i-1 (motifs Ala-Ala, Lys-Lys, Leu-Leu, Asp-Leu, Glu-Leu, Gly-Leu, Lys-Leu, only assigned and non-overlapping peaks) in the recorded ^{1}H-^{15}N SOFAST-HMQC spectra.

All these S/N gains are due to the fact that α/β-deuteration slows down $^{1}H_N$-T2 relaxation, which can be deduced from the observed sharper $^{1}H_N$-linewidths (Fig. 1, Fig. 4A). α/β-deuteration does also affect the apparent interscan $^{1}H_N$-T1* magnetization recovery in ^{1}H-^{15}N SOFAST-HMQC, but not enough to abolish the benefits on the $^{1}H_N$-T2. Interestingly, perdeuteration has a more pronounced effects on $^{1}H_N$-T1*, which has deleterious consequences on S/N-PMUT (Fig. 4B): taking the uniformly protonated form as a reference, p38α perdeuteration decreases $^{1}H_{amide}$ linewidth by ~60–70%, but it also doubles the $^{1}H_N$-R1* (1/T1*) rates.

Finally, our approach using single ^{15}N-labeled amino acids permits to obtain residue-specific information with lower resolution in the ^{1}H- and ^{15}N-dimensions. This has important consequences on the weakest peaks, as seen in Fig. 4B (left), which have apparently the fastest T2 relaxations and greatly benefit from shorter ^{1}H and ^{15}N chemical shift evolutions. Hence, the S/N-PMUTs of p38α integrating $^{2}H_{\alpha/\beta}$-^{15}N amino acids is on average similar to that of the perdeuterated form, especially when supplementary $^{2}H_{\alpha/\beta}$-^{14}N amino acids are present.

Altogether, we reach average S/N-PMUTs of 0.4–0.5 $\mu M^{-1}.h^{-1/2}$ in the ^{1}H-^{15}N SOFAST-HMQC spectra recorded with our $^{2}H_{\alpha/\beta}$-^{15}N-Ala, $^{2}H_{\alpha/\beta}$-^{15}N-Lys or $^{2}H_{10}$-^{15}N-Leu p38α samples (0.2–0.25 $\mu M^{-1}.h^{-1/2}$ at 283 K, data not shown). This is also due to the limited resolution needed to obtain resolved peaks with single ^{15}N-labeled amino acids, which greatly favors S/N-PMUT from ^{1}H-^{15}N SOFAST-HMQC experiments. Interestingly, these S/N-PMUT levels compare rather advantageously with the most sensitive NMR experiment providing residue-specific information, i.e. the ^{1}H-^{13}C SOFAST-methyl-HMQC on perdeuterated proteins integrating ^{1}H-$^{13}C_{\delta1}$-Ile [3,80] (Fig. 4C) (its S/N-PMUT also drops by a factor 2 at 283 K, data not shown). We measured actually similar S/N-PMUTs from our $^{2}H_{\alpha/\beta}$-^{15}N amino acids and from ^{1}H-$^{13}C_{\delta1}$-Ile-residues in the core of p38α (Fig. 4C, Fig. 5D), those that can report for ligand binding in the ATP-pocket or for conformational equilibria, as shown by Shimada and colleagues [61]; at the opposite, the surface Ile-residues are observed at S/N-PMUT levels above 1 and up to ~3 $\mu M^{-1}.h^{-1/2}$ at 700 MHz and 298 K, and provide interesting information regarding protein:protein interactions in vitro [61].

We must underline the fact that we compared ^{1}H-^{15}N SOFAST-HMQC and ^{1}H-^{13}C SOFAST-methyl-HMQC without tuning the excitation pulse to find the Ernst angle offering the maximal sensitivity. This might provide supplementary gains in sensitivity, about 20–40% [57, 80]. Finally, we used 3 mm diameter tubes: the use of 5 mm diameter tubes would naturally yield higher S/N-PMUTs (~ 2-fold).

Application to mapping of p38α's inhibitors binding

We thought to exemplify the benefits of single amino acid labeling coupled to α/β-deuteration for kinase detection and residue-specific characterization by NMR. We show in Fig. 6 the spectra of p38α in presence of two specific inhibitors targeting its enzymatic ATP pocket, namely VX-745 and PH-797804 [81–84]. The homogeneous ^{15}N-labeling asks for a high resolution to deliver residue-specific information, hence requiring the use of a HSQC type of experiments (Fig. 6A). At the opposite, amino acid-specific labeled samples integrating e.g. $^{2}H_{\alpha/\beta}$-^{15}N-Leu or $^{2}H_{\alpha/\beta}$-^{15}N-Lys are much less demanding in resolution to

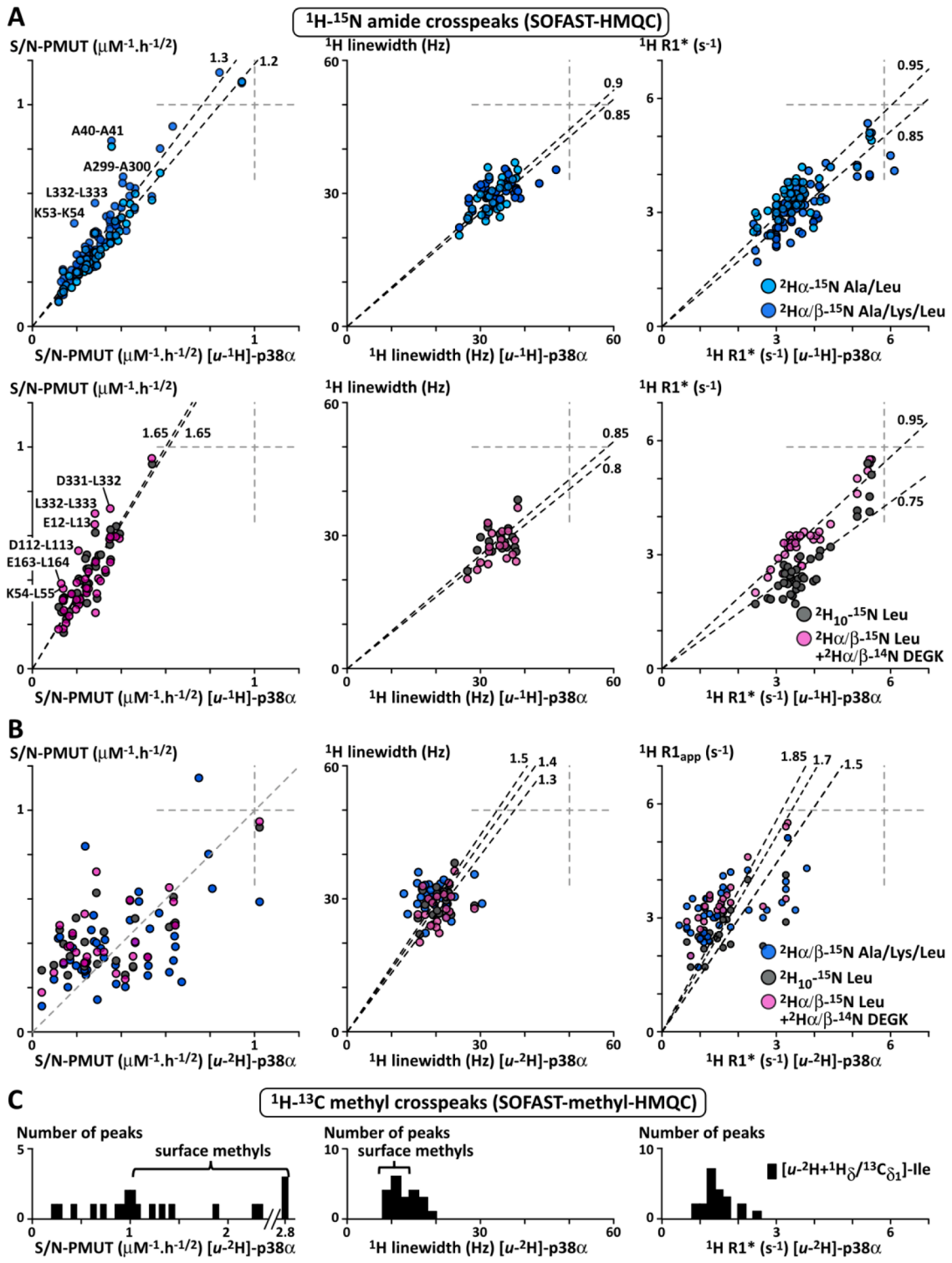

Fig. 4. A. S/N-PMUTs (*left*), $^{1}H_{amide}$-linewidths at half-height (*middle*) and apparent R1*=1/($^{1}H_{N}$-T1*) relaxation rates (*right*) among the well-resolved crosspeaks in two-dimensional ^{1}H-^{15}N SOFAST-HMQC spectra recorded for [*u*-$^{1}H/^{15}N$]-p38α (*abscissa*) and for the various deuterated labeling schemes described on the right (*ordinates*); the dashed lines correspond to the linear regression, the slopes are indicated on top; it is worth noting that Leu-residues start from lower peak intensities than Ala- and Lys- in [*u*-$^{1}H/^{15}N$]-p38α; B. Same as A., but values from [*u*-$^{2}H/^{15}N$]-p38α in abscissa; C. Distributions of S/N-PMUTs, ^{1}H-linewidths at half-height and apparent R1* rates among peaks from two-dimensional ^{1}H-^{13}C SOFAST-methyl-HMQC spectra recorded with [*u*-$^{2}H/^{1}H$-$^{13}C_{\delta1}$-Ile]-p38α. Values in A.-B.-C. were obtained from two independent samples, and from well-separated crosspeaks showing error bars of 15% or less. All samples in A. and B. were produced using cell-free expression in regular H_2O, and transferred in D_2O/H_2O at 97/3 (% v/v), in PBS buffer, hence all amide functions are ~97–100% protonated, depending on their exchange rates. All spectra were recorded in 3 mm diameter tubes, at 298 K and at 700 MHz.

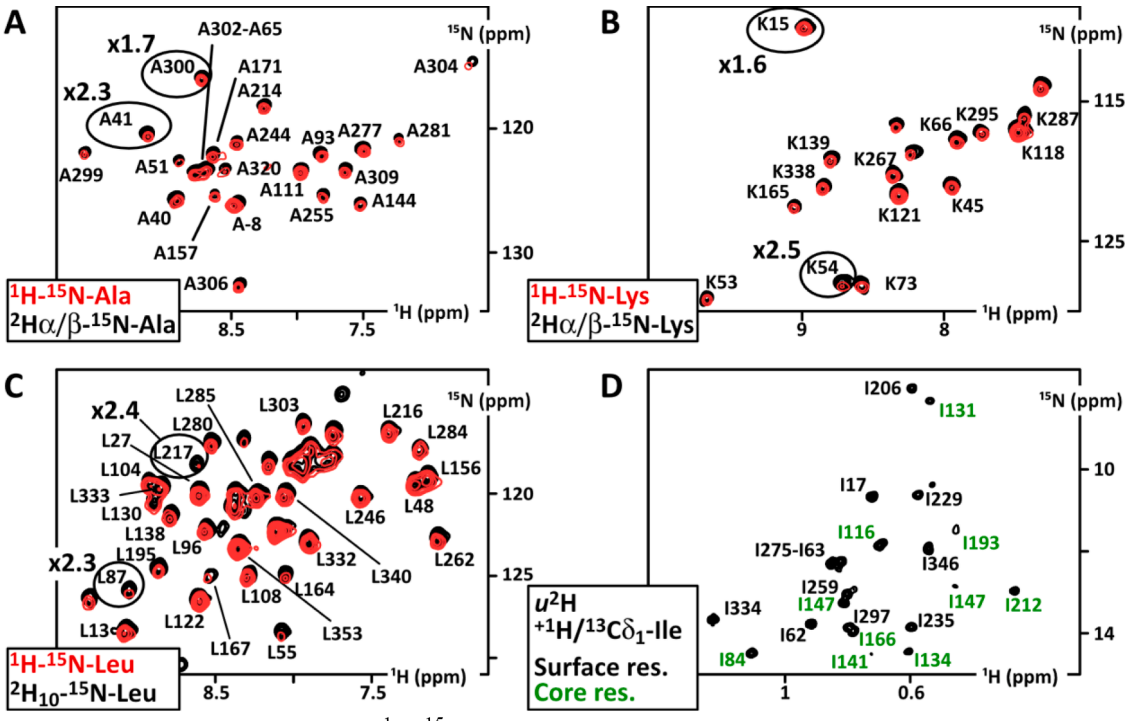

Fig. 5. A. B. C. Overlays of ^{1}H-^{15}N SOFAST-HMQC spectra obtained from p38α integrating ^{15}N-Ala, ^{15}N-Lys or ^{15}N-Leu (red) or ^{2}H$_{α/β}$-^{15}N-Ala, ^{2}H$_{α/β}$-^{15}N-Lys or ^{2}H$_{10}$-^{15}N-Leu (black); the contour levels were adjusted to account for eventual differences in concentrations among the samples; high S/N-PMUT improvements are observed for A40-A41, A299-A300, K53-K54, L86-L87 and L216-L217 motifs. D. ^{1}H-^{13}C SOFAST-methyl-HMQC spectrum of perdeuterated p38α except on ^{1}H-^{13}C$_{δ1}$-Ile-positions, indicating Ile-residues at the surface (black) and those in the core of the structure (green); the first ones can inform on interactions on the surface of p38α, the latter ones about ligand binding and conformation changes [61].

provide well-separated crosspeaks, and thus are adapted to the use of the ^{1}H-^{15}N SOFAST-HMQC (Fig. 6B-C). Similar spectra were also recorded with ^{2}H$_{α/β}$-^{15}N-Ala- or ^{2}H$_{α/β}$-^{15}N-Ser-labeling (Fig. S5). This approach results in important gains in S/N-PMUT, which helps to record valuable spectra in one hour using only 100 μg of kinase (100 μL at 25 μM).

Indeed, ^{2}H$_{α/β}$-^{15}N-Leu- or ^{2}H$_{α/β}$-^{15}N-Lys-labeling schemes generated well-resolved spectra delivering residue-specific information that delineate clearly the ATP pocket as the binding site of VX-745 and PH-797804. We observed also a chemical shift perturbation on Leu195 in the lipid binding pocket of p38α, which may interact loosely with the weak stoichiometric excess of PH-797804. This would be consistent with the fact that this non-ATP site has been reported to accommodate hydrophobic species in a number of crystals [83,85–88].

Discussion

The proton-proton dipolar component of ^{1}H$_N$-T$_2$ relaxation is a dominant cause of signal losses in two-dimensional ^{1}H-^{15}N NMR spectroscopy of proteins at 600–700 MHz. Here, we sought to evaluate experimentally the impact of the sole α- and β-protons on this relaxation, in the context of searching affordable isotopic labeling schemes enhancing NMR sensitivity but avoiding perdeuteration. Selective deuteration would notably find applications in recombinant protein production in eukaryotic cells for NMR purposes. We tested the performances of α- or α-β-deuteration on ^{15}N-Ala, ^{15}N-Lys, ^{15}N-Leu (and also ^{15}N-Ser, which was less straightforward to interpret because of the effects of large water-amide proton exchange, Fig. S6) integrated in the kinase p38α. These were chosen because they were representative, abundant amino acids offering a statistical potential.

We found out that α/β-deuteration of a ^{15}N-labeled amino acid could provoke sensitivity gains of its ^{1}H-^{15}N crosspeak, which are about 20% in the case of Ala- and Leu-, and 40% for Lys-residues. The complete deuteration of Leucine was necessary to reach about 50–60% S/N-PMUT enhancements. The effect of α/β-deuteration in position *i-1* is much larger for ^{1}H-^{15}N$_i$, reaching in a majority of cases 2- to 3-fold enhancements. The introduction of a maximum of ^{2}H$_{α/β}$-^{14}N-amino acids is thus highly advisable, which would marginally increase the production cost. Although ^{2}H$_{α/β}$-amino acids are not yet routinely commercialized, costs of amino acids are in that order: ^{2}H$_{α/β}$-^{14}N < ^{15}N < ^{2}H$_{α/β}$-^{15}N < *u*-^{2}H-^{15}N=*u*-^{2}H-^{14}N (see Table S2, costs for ^{15}N amino acids are about 4 times less than for *u*-^{2}H-^{15}N and *u*-^{2}H-^{14}N amino acids). However, supplemented ^{2}H$_{α/β}$-^{14}N-amino acids should be carefully chosen: as evoked below, not all ^{2}H$_{α/β}$ amino acids can conserve their α-deuteration in living organisms, which can be a source of deleterious heterogeneity in the produced sample.

The amino acid-specific ^{15}N-labeling is actually also highly beneficial for sensitivity, because it permits to record lower resolution ^{1}H-^{15}N spectra that still provide residue-specific information. This makes the SOFAST-HMQC pulse sequence better adapted to the analysis of our model kinase, which yields by itself a 3-fold sensitivity enhancement in comparison to the use of classical HSQC experiments on the uniformly ^{15}N-labeled protein (Fig. 5). This is notably due to the fast restoration of spin polarization, or "apparent T1*" relaxation, enabled by the SOFAST-HMQC scheme [57,73]. Some HSQC and TROSY pulse sequences also use band-selective pulses, which accelerate the longitudinal magnetization and can enhance sensitivity up to factors 2 to 3 [70–75]. These latter ones might compete favorably with the SOFAST-HMQC for studying amino acid specifically ^{2}H$_{α/β}$-^{15}N-labeled proteins, especially for >50 kDa proteins or at higher fields; the opposite trend is expected when increasing the temperature to 310 K. Tuning the angle of excitation and using an Ernst angle in the SOFAST-HMQC scheme might add 20–40% gains in S/N-PMUT [73].

The present approach appears to be an accessible alternative to the strategy considered to offer the highest sensitivity for large proteins, i.e. single ^{1}H/^{13}C-methyl labeling in a perdeuterated background coupled to the detection using ^{1}H-^{13}C SOFAST-methyl-HMQC [3,80]. We observed

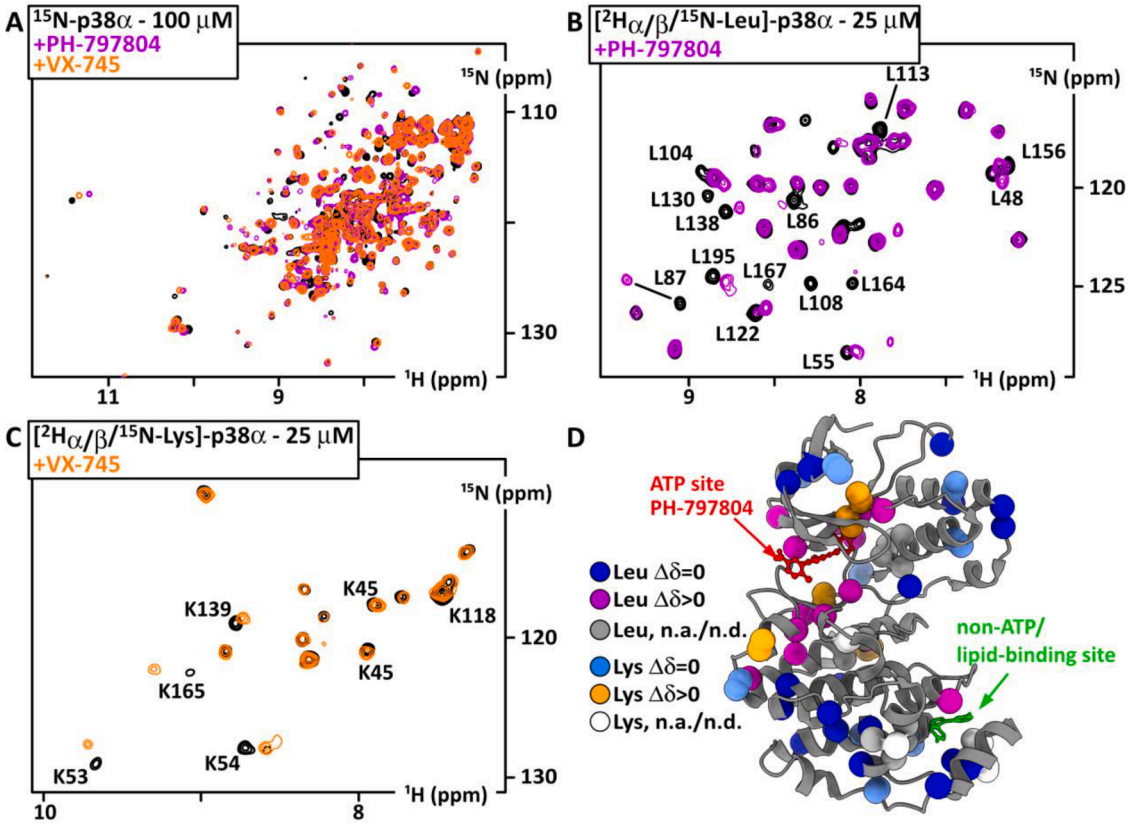

Fig. 6. A. B. C. Two-dimensional ^{1}H-^{15}N spectra corresponding to 1 hour of acquisition, using contours visible from 4 times the average noise level, recorded at 700 MHz and 298 K, in PBS buffer at pH7.4; A. Overlay of ^{1}H-^{15}N seHSQC spectra of ^{15}N-p38α at 100 μM alone (black) or in presence of the inhibitors PH-797804 (magenta) or VX-745 (orange) (1:1.1 stoichiometry for p38α:inhibitor); **B.** Overlay of ^{1}H-^{15}N SOFAST-HMQC spectra of [$^{2}H_{\alpha/\beta}$-^{15}N-Leu]-p38α at 25 μM alone (black) and in presence of PH-797804 (magenta); C. Overlay of ^{1}H-^{15}N SOFAST-HMQC spectra of [$^{2}H_{\alpha/\beta}$-^{15}N-Lys]-p38α at 25 μM alone (black) and in presence of VX-745 (orange); D. Cartoon representation of the crystal structure of p38α in complex with PH-797804 (PDB: 3HLL); balls indicate Leu- and Lys-residues, the purple and orange ones indicating those whose chemical shifts are perturbed in presence of the ligands (n.a.: non assigned; n.d.: non detectable); the ligand PH-797804 is shown in red in the ATP-site; another low-affinity ligand, in green, fills a non-ATP binding pocket, which can accommodate hydrophobic compounds and is found occupied in many crystal structures [83,85–88].

that $^{1}H/^{13}C_{\delta1}$-Ile-labeling generated the highest S/N-PMUT only for surface Ile-residues of p38α, while the ones in the core yielded S/N-PMUTs similar to those observed with our proposed approach, i.e. using amino acid-specific $^{2}H_{\alpha/\beta}$-^{15}N-labeling and ^{1}H-^{15}N SOFAST-HMQC. $^{1}H/^{13}C$-methyl labeling in a perdeuterated background has an average cost of 1500 euros/L in *E. coli* [89]. Its cost in mammalian cells is uncertain: specific $^{1}H/^{13}C$-methyl labeling in such cells will not be achievable by supplementing affordable precursors like in bacteria. Moreover, it will not be possible to combine it with perdeuteration, which compromises mammalian cells growth and viability [19–23]. Without perdeuteration, $^{1}H/^{13}C$-methyl labeling is much less effective in delivering high S/N and well-resolved crosspeaks [30]; a protonated background would probably provoke large signal losses in $^{1}H/^{13}C$ spectra for kinases, probably in the order of magnitude of a 5-fold decrease [3,90–92]. Still, partial deuteration of leucine containing a single ^{1}H-^{13}C-methyl has been proved to yield excellent S/N performances, including upon recombinant production in insect cells [93]. This strategy could probably be implemented with success in mammalian expression systems. ^{1}H-^{15}N correlation experiments is nevertheless promising for NMR studies based on expression in mammalian cells, provided that one uses pulse sequences designed to control the longitudinal relaxation in an optimized fashion [70–75].

To introduce $^{2}H_{\alpha/\beta}$-^{15}N-amino acids in a recombinant p38α, we used here a cell-free expression system avoiding scrambling and back-protonation of deuterated amino acids [46,47,94]. Indeed, amino acid-specific labeling is not always possible in living organisms due to isotopic scrambling, and PLP-dependent enzymes like transaminases often provoke $^{15}N_{amide}$ dilution and H/D exchange in α-positions. Hence, the achievable amino acid-specific labeling schemes depend on the organism chosen for the recombinant production [10,95–98], whose capacities can be expanded in auxotrophic strains designed for this purpose [99,100]. Some isotopically labeled amino acids can be integrated in most organisms with negligible isotopic dilution or alkyl H/D exchange, because they are found at the end of long metabolic chains containing unidirectional steps, e.g. Lys, His, Trp. We are currently testing the introduction of many ^{13}C-, ^{15}N- and $^{2}H_{\alpha/\beta}$-^{15}N-labeled amino acids and precursors thereof in mammalian cells. We intend to use mixes of $^{2}H_{\alpha/\beta}$-^{14}N- and $^{2}H_{\alpha/\beta}$-^{15}N-amino acids to carry out affordable productions of proteins in these cells, and also to generate in-cell NMR samples.

Conclusion

We demonstrated here the potential gains generated by single $^{2}H_{\alpha/\beta}$-^{15}N-amino acid labeling in NMR studies of ~40 kDa proteins like kinases, eventually combined with $^{2}H_{\alpha/\beta}$-^{14}N-amino acids. At 600–700 MHz, this approach can provide S/N-PMUT enhancement about 4–5 when combined with the use of ^{1}H-^{15}N SOFAST-HMQC, as compared to the more common detection of uniform ^{15}N-labeled proteins and standard HSQC or TROSY type of experiments. It can still deliver residue-specific information for characterizing ligand binding or conformational equilibria.

This strategy benefits of the accessible production of $^{2}H_{\alpha/\beta}$ amino acids, using either ruthenium-nanoparticles or enzyme-catalyzed H/D

exchange; among others, we demonstrated that the mutant E352A of CGS makes the α/β deuteration more efficient for amino acids Asp, Glu, Lys, Arg. Our nanoparticles- or enzyme-assisted deuteration methods give access to α- and α/β-deuterated Ala, Asp, Gly, Lys, Leu, Met, Asn, Gln, Ser, Thr, to β-stereoselective α/β-deuterated Glu, His, Arg, and only to α-deuterated Phe, Ile, Pro, Val, Tyr, Trp (see [43], Table S1 and Table S2).

Our approach is readily applicable for cell-free protein expression, but it will also find applications in recombinant production using mammalian cells, which contain less enzymes processing and scrambling amino acids than bacteria.

Declaration of Competing Interest

The authors declare that they have some competing financial interests, but that these have not influenced the work reported in this paper.

Data availability

Data will be made available on request.

Acknowledgments

This work was supported by the CNRS and the CEA-Saclay, by the French Infrastructure for Integrated Structural Biology (https://frisbi.eu/, grant number ANR-10-INSB-05–01, Acronym FRISBI) and by the French National Research Agency (ANR; research grants ANR-14-ACHN-0015 and ANR-20-CE92–0013).

We thank Guy Lippens for suggesting the use of α-deuterated amino acids, and for sharing repeatedly his valuable thoughts through the years.

We thank Philippe Corcos for establishing and supporting the collaboration with Taiyo Nippon Sanso. We also thank the company Taiyo Nippon Sanso for its support in providing Musaibo Kun kits, and we give a special thanks to Takashi Yabuki for his insightful comments and his diligent, tireless support.

Supplementary materials

Supplementary material associated with this article can be found, in the online version, at doi:10.1016/j.jmro.2023.100126.

References

[1] R.A. Venters, B.T. Farmer II, C.A. Fierke, L.D. Spicer, Characterizing the Use of Perdeuteration in NMR Studies of Large Proteins:13C,15N and1H Assignments of Human Carbonic Anhydrase II, J. Mol. Biol. 264 (1996) 1101–1116, https://doi.org/10.1006/jmbi.1996.0699.

[2] K.H. Gardner, L.E. Kay, Tuse of ^{2}H, ^{13}C, ^{15}N multidimensional NMR to study the structure and dynamics of proteins, Annu. Rev. Biophys. Biomol. Struct. 27 (1998) 357–406, https://doi.org/10.1146/annurev.biophys.27.1.357.

[3] S. Schütz, R. Sprangers, Methyl TROSY spectroscopy: a versatile NMR approach to study challenging biological systems, Prog. Nucl. Magn. Reson. Spectrosc. 116 (2020) 56–84, https://doi.org/10.1016/j.pnmrs.2019.09.004.

[4] M. Cai, Y. Huang, R. Yang, R. Craigie, G.M. Clore, A simple and robust protocol for high-yield expression of perdeuterated proteins in Escherichia coli grown in shaker flasks, J. Biomol. NMR. 66 (2016) 85–91, https://doi.org/10.1007/s10858-016-0052-y.

[5] M. Cai, Y. Huang, J. Lloyd, R. Craigie, G.M. Clore, A simple and cost-effective protocol for high-yield expression of deuterated and selectively isoleucine/leucine/valine methyl protonated proteins in Escherichia coli grown in shaker flasks, J. Biomol. NMR. 75 (2021) 83–87, https://doi.org/10.1007/s10858-021-00357-x.

[6] J. Li, R.A. Byrd, A simple protocol for the production of highly deuterated proteins for biophysical studies, J. Biol. Chem. 298 (2022), 102253, https://doi.org/10.1016/j.jbc.2022.102253.

[7] Y. Kofuku, T. Ueda, J. Okude, Y. Shiraishi, K. Kondo, T. Mizumura, S. Suzuki, I. Shimada, Functional Dynamics of Deuterated β 2-Adrenergic Receptor in Lipid Bilayers Revealed by NMR Spectroscopy, Angew. Chem. 53 (2014) 13376–13379, https://doi.org/10.1002/anie.201406603.

[8] A. Meola, C. Deville, S.A. Jeffers, P. Guardado-Calvo, I. Vasiliauskaite, C. Sizun, C. Girard-Blanc, C. Malosse, C. van Heijenoort, J. Chamot-Rooke, T. Krey, E. Guittet, S. Pêtres, F.A. Rey, F. Bontems, Robust and low cost uniform 15N-labeling of proteins expressed in Drosophila S2 cells and Spodoptera frugiperda Sf9 cells for NMR applications, J. Struct. Biol. 188 (2014) 71–78, https://doi.org/10.1016/j.jsb.2014.08.002.

[9] A. Sitarska, L. Skora, J. Klopp, S. Roest, C. Fernández, B. Shrestha, A.D. Gossert, Affordable uniform isotope labeling with 2H, 13C and 15N in insect cells, J. Biomol. NMR. 62 (2015) 191–197, https://doi.org/10.1007/s10858-015-9935-6.

[10] B. Franke, C. Opitz, S. Isogai, A. Grahl, L. Delgado, A.D. Gossert, S. Grzesiek, Production of isotope-labeled proteins in insect cells for NMR, J. Biomol. NMR. 71 (2018) 173–184, https://doi.org/10.1007/s10858-018-0172-7.

[11] Y. Kofuku, T. Yokomizo, S. Imai, Y. Shiraishi, M. Natsume, H. Itoh, M. Inoue, K. Nakata, S. Igarashi, H. Yamaguchi, T. Mizukoshi, E.-I. Suzuki, T. Ueda, I. Shimada, Deuteration and selective labeling of alanine methyl groups of β2-adrenergic receptor expressed in a baculovirus-insect cell expression system, J. Biomol. NMR. 71 (2018) 185–192, https://doi.org/10.1007/s10858-018-0174-5.

[12] C. Opitz, E. Ahrné, K.N. Goldie, A. Schmidt, S. Grzesiek, Deuterium induces a distinctive Escherichia coli proteome that correlates with the reduction in growth rate, J. Biol. Chem. 294 (2019) 2279–2292, https://doi.org/10.1074/jbc.RA118.006914.

[13] E. Flaumenhaft, S. Bose, H.L. Crespi, J.J. Katz, Deuterium Isotope Effects in Cytology. Int. Rev. Cytol., Elsevier, 1965, pp. 313–361, https://doi.org/10.1016/S0074-7696(08)60557-4.

[14] J.J. Katz, H.L. Crespi, Deuterated Organisms: cultivation and Uses: living organisms of unusual isotopic composition can be used for magnetic resonance studies, Science 151 (1966) 1187–1194, https://doi.org/10.1126/science.151.3715.1187.

[15] V. Kselíková, M. Vítová, K. Bišová, Deuterium and its impact on living organisms, Folia Microbiol. (Praha). 64 (2019) 673–681, https://doi.org/10.1007/s12223-019-00740-0.

[16] M. Sastry, L. Xu, I.S. Georgiev, C.A. Bewley, G.J. Nabel, P.D. Kwong, Mammalian production of an isotopically enriched outer domain of the HIV-1 gp120 glycoprotein for NMR spectroscopy, J. Biomol. NMR. 50 (2011) 197–207, https://doi.org/10.1007/s10858-011-9506-4.

[17] S. Kubo, N. Nishida, Y. Udagawa, O. Takarada, S. Ogino, I. Shimada, A gel-encapsulated bioreactor system for NMR studies of protein-protein interactions in living mammalian cells, Angew. Chem. Int. Ed Engl. 52 (2013) 1208–1211, https://doi.org/10.1002/anie.201207243.

[18] F.-X. Theillet, In-Cell Structural Biology by NMR: the Benefits of the Atomic Scale, Chem. Rev. 122 (2022) 9497–9570, https://doi.org/10.1021/acs.chemrev.1c00937.

[19] J. Murphy, C. Desaive, W. Giaretti, F. Kendall, C. Nicolini, Experimental results on mammalian cells growing in vitro in deuterated medium for neutron-scattering studies, J. Cell Sci. 25 (1977) 87–94, https://doi.org/10.1242/jcs.25.1.87.

[20] H. Takeda, Y. Nio, H. Omori, K. Uegaki, N. Hirahara, S. Sasaki, K. Tamura, H. Ohtani, Mechanisms of cytotoxic effects of heavy water (deuterium oxide: D20) on cancer cells, Anticancer. Drugs. 9 (1998) 715–725, https://doi.org/10.1097/00001813-199809000-00007.

[21] A. Mandegary, E. Sharif, R. Rasooli, A. Hassanzadeh, The effect of deuterium depleted/enriched water on the growth of A549 and HepG2 cell lines, J. Kerman Univ. Med. Sci. (2019) 26, https://doi.org/10.22062/jkmu.2019.89543.

[22] J. Kleemann, G. Reichenbach, N. Zöller, M. Jäger, R. Kaufmann, M. Meissner, S. Kippenberger, Heavy water affects vital parameters of human melanoma cells in vitro, Cancer Manag. Res. Volume 12 (2020) 1199–1209, https://doi.org/10.2147/CMAR.S230985.

[23] J. Jandova, A.B. Hua, J. Fimbres, G.T. Wondrak, Deuterium oxide (D2O) induces early stress response gene expression and impairs growth and metastasis of experimental malignant melanoma, Cancers (Basel) 13 (2021) 605, https://doi.org/10.3390/cancers13040605.

[24] S.-E. Ong, B. Blagoev, I. Kratchmarova, D.B. Kristensen, H. Steen, A. Pandey, M. Mann, Stable isotope labeling by amino acids in cell culture, SILAC, as a simple and accurate approach to expression proteomics, Mol. Cell. Proteomics. 1 (2002) 376–386, https://doi.org/10.1074/mcp.M200025-MCP200.

[25] S.-E. Ong, G. Mittler, M. Mann, Identifying and quantifying in vivo methylation sites by heavy methyl SILAC, Nat. Methods. 1 (2004) 119–126, https://doi.org/10.1038/nmeth715.

[26] F.W. Pagliuca, M.O. Collins, A. Lichawska, P. Zegerman, J.S. Choudhary, J. Pines, Quantitative proteomics reveals the basis for the biochemical specificity of the cell-cycle machinery, Mol. Cell. 43 (2011) 406–417, https://doi.org/10.1016/j.molcel.2011.05.031.

[27] Z. Wu, C.H. Na, H. Tan, J. Peng, Global Ubiquitination Analysis by SILAC in Mammalian Cells, in: B. Warscheid (Ed.), Stable Isot. Labeling Amino Acids Cell Cult. SILAC, Springer New York, New York, NY, 2014, pp. 149–160, https://doi.org/10.1007/978-1-4939-1142-4_11.

[28] M. Kaller, S. Oeljeklaus, B. Warscheid, H. Hermeking, Identification of MicroRNA Targets by Pulsed SILAC, in: B. Warscheid (Ed.), Stable Isot. Labeling Amino Acids Cell Cult. SILAC, Springer New York, New York, NY, 2014, pp. 327–349, https://doi.org/10.1007/978-1-4939-1142-4_23.

[29] X. Chen, S. Wei, Y. Ji, X. Guo, F. Yang, Quantitative proteomics using SILAC: principles, applications, and developments, Proteomics 15 (2015) 3175–3192, https://doi.org/10.1002/pmic.201500108.

[30] S. Yanaka, H. Yagi, R. Yogo, M. Yagi-Utsumi, K. Kato, Stable isotope labeling approaches for NMR characterization of glycoproteins using eukaryotic

expression systems, J. Biomol. NMR. 71 (2018) 193–202, https://doi.org/10.1007/s10858-018-0169-2.
[31] C. Fuccio, E. Luchinat, L. Barbieri, S. Neri, M. Fragai, Algal autolysate medium to label proteins for NMR in mammalian cells, J. Biomol. NMR. 64 (2016) 275–280, https://doi.org/10.1007/s10858-016-0026-0.
[32] L. Barbieri, E. Luchinat, L. Banci, Characterization of proteins by in-cell NMR spectroscopy in cultured mammalian cells, Nat. Protoc. 11 (2016) 1101–1111, https://doi.org/10.1038/nprot.2016.061.
[33] S. Yanaka, H. Yagi, R. Yogo, M. Onitsuka, K. Kato, Glutamine-free mammalian expression of recombinant glycoproteins with uniform isotope labeling: an application for NMR analysis of pharmaceutically relevant Fc glycoforms of human immunoglobulin G1, J. Biomol. NMR. 76 (2022) 17–22, https://doi.org/10.1007/s10858-021-00387-5.
[34] M. Hunter, P. Yuan, D. Vavilala, M. Fox, Optimization of protein expression in mammalian cells, Curr. Protoc. Protein Sci. 95 (2019) e77, https://doi.org/10.1002/cpps.77.
[35] G.O. Krasnoselska, M. Dumoux, N. Gamage, H. Cheruvara, J. Birch, A. Quigley, R. J. Owens, Transient transfection and expression of eukaryotic membrane proteins in Expi293F cells and their screening on a small scale: application for structural studies, in: R.J. Owens (Ed.), Struct. Proteomics, Springer US, New York, NY, 2021, pp. 105–128, https://doi.org/10.1007/978-1-0716-1406-8_5.
[36] B. Tihanyi, L. Nyitray, Recent advances in CHO cell line development for recombinant protein production, Drug Discov. Today Technol. (2021), S1740674921000068, https://doi.org/10.1016/j.ddtec.2021.02.003.
[37] M. Pulix, V. Lukashchuk, D.C. Smith, A.J. Dickson, Molecular characterization of HEK293 cells as emerging versatile cell factories, Curr. Opin. Biotechnol. 71 (2021) 18–24, https://doi.org/10.1016/j.copbio.2021.05.001.
[38] F.-X. Theillet, E. Luchinat, In-cell NMR: why and how? Prog. Nucl. Magn. Reson. Spectrosc. 132–133 (2022) 1–112, https://doi.org/10.1016/j.pnmrs.2022.04.002.
[39] Y. Kofuku, T. Ueda, J. Okude, Y. Shiraishi, K. Kondo, M. Maeda, H. Tsujishita, I. Shimada, Efficacy of the β2-adrenergic receptor is determined by conformational equilibrium in the transmembrane region, Nat. Commun. 3 (2012) 1045–1049, https://doi.org/10.1038/ncomms2046.
[40] J. Okude, T. Ueda, Y. Kofuku, M. Sato, N. Nobuyama, K. Kondo, Y. Shiraishi, T. Mizumura, K. Onishi, M. Natsume, M. Maeda, H. Tsujishita, T. Kuranaga, M. Inoue, I. Shimada, Identification of a conformational equilibrium that determines the efficacy and functional selectivity of the μ-opioid receptor, Angew. Chem. Int. Ed Engl. 54 (2015) 15771–15776, https://doi.org/10.1002/anie.201508794.
[41] S. Imai, T. Yokomizo, Y. Kofuku, Y. Shiraishi, T. Ueda, I. Shimada, Structural equilibrium underlying ligand-dependent activation of β2-adrenoreceptor, Nat. Chem. Biol. 16 (2020) 430–439, https://doi.org/10.1038/s41589-019-0457-5.
[42] B. Canovas, A.R. Nebreda, Diversity and versatility of p38 kinase signalling in health and disease, Nat. Rev. Mol. Cell Biol. (2021) 1–21, https://doi.org/10.1038/s41580-020-00322-w.
[43] R.J. Homer, M.S. Kim, D.M. LeMaster, The use of cystathionine gamma-synthase in the production of alpha and chiral beta deuterated amino acids, Anal. Biochem. 215 (1993) 211–215, https://doi.org/10.1006/abio.1993.1577.
[44] A. Michelotti, F. Rodrigues, M. Roche, Development and scale-up of stereoretentive α-deuteration of amines, Org. Process Res. Amp Dev. 21 (2017) 1741–1744, https://doi.org/10.1021/acs.oprd.7b00227.
[45] C. Taglang, L.M. Martínez-Prieto, I. del Rosal, L. Maron, R. Poteau, K. Philippot, B. Chaudret, S. Perato, A.S. Lone, C. Puente, C. Dugave, B. Rousseau, G. Pieters, Enantiospecific C-H activation using ruthenium nanocatalysts, Angew. Chem. 127 (2015) 10620–10623, https://doi.org/10.1002/ange.201504554.
[46] J. Yokoyama, T. Matsuda, S. Koshiba, N. Tochio, T. Kigawa, A practical method for cell-free protein synthesis to avoid stable isotope scrambling and dilution, Anal. Biochem. 411 (2011) 223–229, https://doi.org/10.1016/j.ab.2011.01.017.
[47] B. Hoffmann, F. Lohr, A. LaGuerre, F. Bernhard, V. Dötsch, Protein labeling strategies for liquid-state NMR spectroscopy using cell-free synthesis, Prog. Nucl. Magn. Reson. Spectrosc. 105 (2018) 1–22, https://doi.org/10.1016/j.pnmrs.2017.11.004.
[48] D.S. Wishart, C.G. Bigam, J. Yao, F. Abildgaard, H.J. Dyson, E. Oldfield, J. L. Markley, B.D. Sykes, 1H, 13C and 15N chemical shift referencing in biomolecular NMR, J. Biomol. NMR. 6 (1995) 135–140, https://doi.org/10.1007/BF00211777.
[49] M.H. Levitt, Spin Dynamics, John Wiley & Sons Ltd, Chichester, 2008. https://www.wiley.com/en-fr/Spin+Dynamics:+Basics+of+Nuclear+Magnetic+Resonance,+2nd+Edition-p-9780470511176.
[50] S. Chhabra, P. Fischer, K. Takeuchi, A. Dubey, J.J. Ziarek, A. Boeszoermenyi, D. Mathieu, W. Bermel, N.E. Davey, G. Wagner, H. Arthanari, 15N detection harnesses the slow relaxation property of nitrogen: delivering enhanced resolution for intrinsically disordered proteins, Proc. Natl. Acad. Sci. 115 (2018) E1710–E1719, https://doi.org/10.1073/pnas.1717560115.
[51] T. Kigawa, T. Yabuki, N. Matsuda, T. Matsuda, R. Nakajima, A. Tanaka, S. Yokoyama, Preparation of Escherichia coli cell extract for highly productive cell-free protein expression, J. Struct. Funct. Genomics. 5 (2004) 63–68, https://doi.org/10.1023/B:JSFG.0000029204.57846.7d.
[52] T. Matsuda, S. Koshiba, N. Tochio, E. Seki, N. Iwasaki, T. Yabuki, M. Inoue, S. Yokoyama, T. Kigawa, Improving cell-free protein synthesis for stable-isotope labeling, J. Biomol. NMR. 37 (2007) 225–229, https://doi.org/10.1007/s10858-006-9127-5.
[53] E. Seki, N. Matsuda, S. Yokoyama, T. Kigawa, Cell-free protein synthesis system from Escherichia coli cells cultured at decreased temperatures improves productivity by decreasing DNA template degradation, Anal. Biochem. 377 (2008) 156–161, https://doi.org/10.1016/j.ab.2008.03.001.
[54] J. Yokoyama, T. Matsuda, S. Koshiba, T. Kigawa, An economical method for producing stable-isotope labeled proteins by the E. coli cell-free system, J. Biomol. NMR. 48 (2010) 193–201, https://doi.org/10.1007/s10858-010-9455-3.
[55] K. Higuchi, T. Yabuki, M. Ito, T. Kigawa, Cold shock proteins improve *E. coli* cell-free synthesis in terms of soluble yields of aggregation-prone proteins, Biotechnol. Bioeng. 117 (2020) 1628–1639, https://doi.org/10.1002/bit.27326.
[56] A.R. Gruber, R. Lorenz, S.H. Bernhart, R. Neubock, I.L. Hofacker, The Vienna RNA Websuite, Nucleic Acids Res. 36 (2008) W70–W74, https://doi.org/10.1093/nar/gkn188.
[57] P. Schanda, Ē. Kupče, B. Brutscher, SOFAST-HMQC experiments for recording two-dimensional heteronuclear correlation spectra of proteins within a few seconds, J. Biomol. NMR. 33 (2005) 199–211, https://doi.org/10.1007/s10858-005-4425-x.
[58] M. Vogtherr, K. Saxena, S. Grimme, M. Betz, U. Schieborr, B. Pescatore, T. Langer, H. Schwalbe, NMR backbone assignment of the mitogen-activated protein (MAP) kinase p38, J. Biomol. NMR. 32 (2005) 175, https://doi.org/10.1007/s10858-005-2449-x.
[59] G. Nielsen, H. Schwalbe, NMR spectroscopic investigations of the activated p38α mitogen-activated protein kinase, ChemBioChem 12 (2011) 2599–2607, https://doi.org/10.1002/cbic.201100527.
[60] D.M. Francis, B. Różycki, D. Koveal, G. Hummer, R. Page, W. Peti, Structural basis of p38α regulation by hematopoietic tyrosine phosphatase, Nat. Chem. Biol. 7 (2011) 916–924, https://doi.org/10.1038/nchembio.707.
[61] Y. Tokunaga, K. Takeuchi, H. Takahashi, I. Shimada, Allosteric enhancement of MAP kinase p38α's activity and substrate selectivity by docking interactions, Nat. Struct. Mol. Biol. 21 (2014) 704–711, https://doi.org/10.1038/nsmb.2861.
[62] J. Schleucher, M. Schwendinger, M. Sattler, P. Schmidt, O. Schedletzky, S. J. Glaser, O.W. S◆rensen, C. Griesinger, A general enhancement scheme in heteronuclear multidimensional NMR employing pulsed field gradients, J. Biomol. NMR. 4 (1994), https://doi.org/10.1007/BF00175254.
[63] T. Schulte-Herbrüggen, O.W. Sørensen, Clean TROSY: compensation for relaxation-induced artifacts, J. Magn. Reson. 144 (2000) 123–128, https://doi.org/10.1006/jmre.2000.2020.
[64] P.C. Aoto, R.L. Stanfield, I.A. Wilson, H.J. Dyson, P.E. Wright, A dynamic switch in inactive p38γ leads to an excited state on the pathway to an active kinase, Biochemistry 58 (2019) 5160–5172, https://doi.org/10.1021/acs.biochem.9b00932.
[65] M. Czisch, R. Boelens, Sensitivity enhancement in the TROSY experiment, J. Magn. Reson. 134 (1998) 158–160, https://doi.org/10.1006/jmre.1998.1483.
[66] K.V. Pervushin, G. Wider, K. Wüthrich, Single Transition-to-single Transition Polarization Transfer (ST2-PT) in [15N,1H]-TROSY, J. Biomol. NMR. 12 (1998) 345–348, https://doi.org/10.1023/A:1008268930690.
[67] G. Zhu, X.M. Kong, K.H. Sze, Gradient and sensitivity enhancement of 2D TROSY with water flip-back, 3D NOESY-TROSY and TOCSY-TROSY experiments, J. Biomol. NMR. 13 (1999) 77–81, https://doi.org/10.1023/A:1008398227519.
[68] D. Nietlispach, Suppression of anti-TROSY lines in a sensitivity enhanced gradient selection TROSY scheme, J. Biomol. NMR. 31 (2005) 161–166, https://doi.org/10.1007/s10858-004-8195-7.
[69] R.R.P. Senthamarai, I. Kuprov, K. Pervushin, Benchmarking NMR experiments: a relational database of protein pulse sequences, J. Magn. Reson. 203 (2010) 129–137, https://doi.org/10.1016/j.jmr.2009.12.008.
[70] R. Riek, Enhancement of the steady-state magnetization in TROSY experiments, J. Biomol. NMR. 21 (2001) 99–105, https://doi.org/10.1023/a:1012431013082.
[71] K. Pervushin, B. Vögeli, A. Eletsky, Longitudinal 1H Relaxation Optimization in TROSY NMR Spectroscopy, J. Am. Chem. Soc. 124 (2002) 12898–12902, https://doi.org/10.1021/ja027149q.
[72] J. Farjon, J. Boisbouvier, P. Schanda, A. Pardi, J.-P. Simorre, B. Brutscher, Longitudinal-relaxation-enhanced NMR experiments for the study of nucleic acids in solution, J. Am. Chem. Soc. 131 (2009) 8571–8577, https://doi.org/10.1021/ja901633y.
[73] Paul Schanda, Fast-pulsing longitudinal relaxation optimized techniques: enriching the toolbox of fast biomolecular NMR spectroscopy, Prog. Nucl. Magn. Reson. Spectrosc. 55 (2009) 238–265, https://doi.org/10.1016/j.pnmrs.2009.05.002.
[74] E. Lescop, T. Kern, B. Brutscher, Guidelines for the use of band-selective radiofrequency pulses in hetero-nuclear NMR: example of longitudinal-relaxation-enhanced BEST-type 1H–15N correlation experiments, J. Magn. Reson. 203 (2010) 190–198, https://doi.org/10.1016/j.jmr.2009.12.001.
[75] A. Favier, B. Brutscher, Recovering lost magnetization: polarization enhancement in biomolecular NMR, J. Biomol. NMR. 49 (2011) 9–15, https://doi.org/10.1007/s10858-010-9461-5.
[76] M. Billeter, W. Braun, K. Wüthrich, Sequential resonance assignments in protein 1H nuclear magnetic resonance spectra, J. Mol. Biol. 155 (1982) 321–346, https://doi.org/10.1016/0022-2836(82)90008-0.
[77] H.J. Dyson, P.E. Wright, Defining solution conformations of small linear peptides, Annu. Rev. Biophys. Biophys. Chem. 20 (1991) 519–538, https://doi.org/10.1146/annurev.bb.20.060191.002511.
[78] S.S. Taylor, A.P. Kornev, Protein kinases: evolution of dynamic regulatory proteins, Trends Biochem. Sci. 36 (2011) 65–77, https://doi.org/10.1016/j.tibs.2010.09.006.

[79] M.M. Attwood, D. Fabbro, A.V. Sokolov, S. Knapp, H.B. Schiöth, Trends in kinase drug discovery: targets, indications and inhibitor design, Nat. Rev. Drug Discov. 20 (2021) 839–861, https://doi.org/10.1038/s41573-021-00252-y.

[80] C. Amero, P. Schanda, M.A. Durá, I. Ayala, D. Marion, B. Franzetti, B. Brutscher, J. Boisbouvier, Fast two-dimensional NMR spectroscopy of high molecular weight protein assemblies, J. Am. Chem. Soc. 131 (2009) 3448–3449, https://doi.org/10.1021/ja809880p.

[81] L. Xing, H.S. Shieh, S.R. Selness, R.V. Devraj, J.K. Walker, B. Devadas, H.R. Hope, R.P. Compton, J.F. Schindler, J.L. Hirsch, A.G. Benson, R.G. Kurumbail, R. A. Stegeman, J.M. Williams, R.M. Broadus, Z. Walden, J.B. Monahan, Structural bioinformatics-based prediction of exceptional selectivity of p38 MAP kinase inhibitor PH-797804, Biochemistry 48 (2009) 6402–6411, https://doi.org/10.1021/bi900655f.

[82] R. Azevedo, M. van Zeeland, H. Raaijmakers, B. Kazemier, J. de Vlieg, A. Oubrie, X-ray structure of p38α bound to TAK-715: comparison with three classic inhibitors, Acta Crystallogr. D Biol. Crystallogr. 68 (2012) 1041–1050, https://doi.org/10.1107/S090744491201997X.

[83] C. Yueh, J. Rettenmaier, B. Xia, D.R. Hall, A. Alekseenko, K.A. Porter, K. Barkovich, G. Keseru, A. Whitty, J.A. Wells, S. Vajda, D. Kozakov, Kinase Atlas: druggability analysis of potential allosteric sites in kinases, J. Med. Chem. 62 (2019) 6512–6524, https://doi.org/10.1021/acs.jmedchem.9b00089.

[84] M.M. Madkour, H.S. Anbar, M.I. El-Gamal, Current status and future prospects of p38α/MAPK14 kinase and its inhibitors, Eur. J. Med. Chem. 213 (2021), 113216, https://doi.org/10.1016/j.ejmech.2021.113216.

[85] R. Diskin, D. Engelberg, O. Livnah, A novel lipid binding site formed by the MAP Kinase Insert in p38α, J. Mol. Biol. 375 (2008) 70–79, https://doi.org/10.1016/j.jmb.2007.09.002.

[86] K.M. Comess, C. Sun, C. Abad-Zapatero, E.R. Goedken, R.J. Gum, D.W. Borhani, M. Argiriadi, D.R. Groebe, Y. Jia, J.E. Clampit, D.L. Haasch, H.T. Smith, S. Wang, D. Song, M.L. Coen, T.E. Cloutier, H. Tang, X. Cheng, C. Quinn, B. Liu, Z. Xin, G. Liu, E.H. Fry, V. Stoll, T.I. Ng, D. Banach, D. Marcotte, D.J. Burns, D. J. Calderwood, P.J. Hajduk, Discovery and characterization of Non-ATP site inhibitors of the mitogen activated protein (MAP) kinases, ACS Chem. Biol. 6 (2011) 234–244, https://doi.org/10.1021/cb1002619.

[87] N. Tzarum, Y. Eisenberg-Domovich, J.J. Gills, P.A. Dennis, O. Livnah, Lipid molecules induce p38α activation via a novel molecular switch, J. Mol. Biol. 424 (2012) 339–353, https://doi.org/10.1016/j.jmb.2012.10.007.

[88] A. Astolfi, G. Manfroni, V. Cecchetti, M.L. Barreca, A comprehensive structural overview of p38α mitogen-activated protein kinase in complex with ATP-site and non-ATP-site binders, ChemMedChem 13 (2018) 7–14, https://doi.org/10.1002/cmdc.201700636.

[89] A.C. McShan, Utility of methyl side chain probes for solution NMR studies of large proteins, J. Magn. Reson. Open. 14–15 (2023), 100087, https://doi.org/10.1016/j.jmro.2022.100087.

[90] P.J. Hajduk, D.J. Augeri, J. Mack, R. Mendoza, J. Yang, S.F. Betz, S.W. Fesik, NMR-based screening of proteins containing ^{13}C-labeled methyl groups, J. Am. Chem. Soc. 122 (2000) 7898–7904, https://doi.org/10.1021/ja000350l.

[91] V. Tugarinov, P.M. Hwang, J.E. Ollerenshaw, L.E. Kay, Cross-correlated relaxation enhanced ^{1}H– ^{13}C NMR spectroscopy of methyl groups in very high molecular weight proteins and protein complexes, J. Am. Chem. Soc. 125 (2003) 10420–10428, https://doi.org/10.1021/ja030153x.

[92] V. Tugarinov, L.E. Kay, An isotope labeling strategy for methyl TROSY spectroscopy, J. Biomol. NMR. 28 (2004) 165–172, https://doi.org/10.1023/B:JNMR.0000013824.93994.1f.

[93] A. Dubey, N. Stoyanov, T. Viennet, S. Chhabra, S. Elter, J. Borggräfe, A. Viegas, R. P. Nowak, N. Burdzhiev, O. Petrov, E.S. Fischer, M. Etzkorn, V. Gelev, H. Arthanari, Local deuteration enables NMR observation of methyl groups in proteins from eukaryotic and cell-free expression systems, Angew. Chem. Int. Ed. Engl. 60 (2021) 13783–13787, https://doi.org/10.1002/anie.202016070.

[94] L. Imbert, R. Lenoir-Capello, E. Crublet, A. Vallet, R. Awad, I. Ayala, C. Juillan-Binard, H. Mayerhofer, R. Kerfah, P. Gans, E. Miclet, J. Boisbouvier, In vitro production of perdeuterated proteins in H2O for biomolecular NMR studies, in: Y. W. Chen, C.-P.B. Yiu (Eds.), Struct. Genomics, Springer US, New York, NY, 2021, pp. 127–149, https://doi.org/10.1007/978-1-0716-0892-0_8.

[95] D. Lacabanne, B.H. Meier, A. Böckmann, Selective labeling and unlabeling strategies in protein solid-state NMR spectroscopy, J. Biomol. NMR. 71 (2018) 141–150, https://doi.org/10.1007/s10858-017-0156-z.

[96] Y. Zhang, H. Wei, D. Xie, D. Calambur, A. Douglas, M. Gao, F. Marsilio, W. J. Metzler, N. Szapiel, P. Zhang, M.R. Witmer, L. Mueller, D. Hedin, An improved protocol for amino acid type-selective isotope labeling in insect cells, J. Biomol. NMR. 68 (2017) 237–247, https://doi.org/10.1007/s10858-017-0117-6.

[97] K. Lee, J.H. Lee, Stable isotope labeling of proteins in mammalian cells, J. Korean Magn. Reson. Soc. 24 (2020) 77–85, https://doi.org/10.6564/JKMRS.2020.24.3.077.

[98] M. Zhang, Recent developments of methyl-labeling strategies in Pichia pastoris for NMR spectroscopy, Protein Expr. Purif. 166 (2020), 105521, https://doi.org/10.1016/j.pep.2019.105521.

[99] T. Iwasaki, Y. Miyajima-Nakano, R. Fukazawa, M.T. Lin, S. Matsushita, E. Hagiuda, A.T. Taguchi, S.A. Dikanov, Y. Oishi, R.B. Gennis, *Escherichia coli* amino acid auxotrophic expression host strains for investigating protein structure–function relationships, J. Biochem. (Tokyo). 169 (2021) 387–394, https://doi.org/10.1093/jb/mvaa140.

[100] P. Rossi, Y.R. Monneau, Y. Xia, Y. Ishida, C.G. Kalodimos, Toolkit for NMR studies of methyl-labeled proteins. Methods Enzymol., Elsevier, 2019, pp. 107–142, https://doi.org/10.1016/bs.mie.2018.08.036.